nature structural & molecular biology

The snake venom protein botrocetin acts as a biological brace to promote dysfunctional platelet aggregation

Koichi Fukuda[1], Teresa Doggett[2,4], Ian J Laurenzi[3,4], Robert C Liddington[1] & Thomas G Diacovo[2]

Botrocetin is a snake venom protein that enhances the affinity of the A1 domain of plasma von Willebrand factor (vWF) for the platelet receptor glycoprotein Ibα (GPIbα), an event that contributes to bleeding and host death. Here we describe a kinetic and crystallographic analysis of this interaction that reveals a novel mechanism of affinity enhancement. Using high-temporal-resolution microscopy, we show that botrocetin decreases the GPIbα off-rate two-fold in both human and mouse complexes without affecting the on-rate. The key to this behavior is that, upon binding of GPIbα to vWF-A1, botrocetin prebound to vWF-A1 makes no contacts initially with GPIbα, but subsequently slides around the A1 surface to form a new interface. This two-step mechanism and flexible coupling may prevent adverse alterations in on-rate of GPIbα for vWF-A1, and permit adaptation to structural differences in GPIbα and vWF in several prey species.

The ability of platelets to tether transiently to the surface of injured vessels before firm adhesion requires the rapid formation and breakage of bonds formed between GPIbα and the A1 domain of vWF[1–3]. This process relies on the ability of vWF, a multidomain, multimeric plasma protein, to form a bridge between platelets and the region of vascular injury. Under physiological conditions, platelets and vWF do not interact appreciably in circulating blood, thus restricting adhesion to sites of vascular damage. This tightly regulated interaction can be perturbed, however, by botrocetin, a component of *Bothrops jararaca* venom that promotes platelet-vWF agglutination in several mammalian species under hemodynamic conditions that typically preclude this event from occurring (such as low-flow states). The consequence of this enhancement in adhesion, in conjunction with the activities of other procoagulant factors contained within the venom, is the loss of vWF multimers and a reduction in platelet counts, resulting in hemorrhage[4–6].

It has been proposed that botrocetin regulates the activity of vWF allosterically, by altering the structure of GPIbα binding surface on the A1 domain. This hypothesis is supported by the requirement of botrocetin to first form a tight binary complex with the A1 domain to enhance its interaction with GPIbα in stasis[4,7,8]. Further support is provided by the ability of botrocetin to 'reconstitute' the binding activity of vWF-A1 containing loss-of-function mutations associated with type 2M von Willebrand disease (vWD) in fluid-phase assays[9,10]. By contrast, our previous analysis of the crystal structure of the human vWF-A1–botrocetin binary complex did not indicate a conformational change induced in A1 by the binding of botrocetin, leading us to suggest that botrocetin enhances GPIbα interactions by providing an additional binding surface[11]. However, this could not be confirmed by simple modeling of the ternary botrocetin–vWF-A1–GPIbα complex based on the botrocetin–vWF-A1 and vWF-A1–GPIbα[12] binary complexes, because no direct contacts are evident between GPIbα and botrocetin. Thus, the mechanism of affinity enhancement was unclear, as was the mechanism by which botrocetin is able to perturb hemostasis in several prey species[4].

We therefore determined the crystal structures of the binary mouse A1–botrocetin complex and the human ternary complex, and evaluated kinetic properties of both species under hydrodynamic conditions. Our data reveal a novel mechanism that provides the adaptability required to recognize different species, and new insights into the mechanisms by which the kinetics of the interaction between GPIbα and vWF-A1 can be altered.

RESULTS

Structure of the mouse A1–botrocetin binary complex

To shed light on the ability of botrocetin to 'activate' vWF such that it enhances its interaction with platelets, we first determined the crystal structure of the mouse A1–botrocetin binary complex at a resolution of 2.7 Å (**Fig. 1**) and compared it with the human binary complex already determined (PDB entry 1IJK)[11]. Mouse A1 is 86% identical to human, and the sequence is highly conserved (81–90%) in the 26 other mammalian species that have been sequenced[13]. The central β-sheets of the Rossmann-like fold superimpose very closely (r.m.s. deviation, 0.33 Å), whereas the overall r.m.s. deviation is 0.75 Å for the 194 equivalent Cα atom pairs. Botrocetin engages helices α5 and α6 on one side of the A1 domain, and side chains that form the botrocetin-binding surface are essentially invariant. However, differences in residues that define the

[1]Infectious and Inflammatory Disease Center, The Burnham Institute, 10901 North Torrey Pines Road, La Jolla, California 92037, USA. [2]Department of Pediatrics and Pathology, Washington University School of Medicine, 660 South Euclid Avenue, St. Louis, Missouri 63110, USA. [3]Department of Molecular Biophysics and Biochemistry, Yale University, Bass 437, 266 Whitney Avenue, New Haven, Connecticut 06520, USA. [4]These authors contributed equally to this work. Correspondence should be addressed to T.G.D. (diacovo_t@kids.wustl.edu) or R.C.L. (rlidding@burnham.org).

Published online 16 January 2005; doi:10.1038/nsmb892

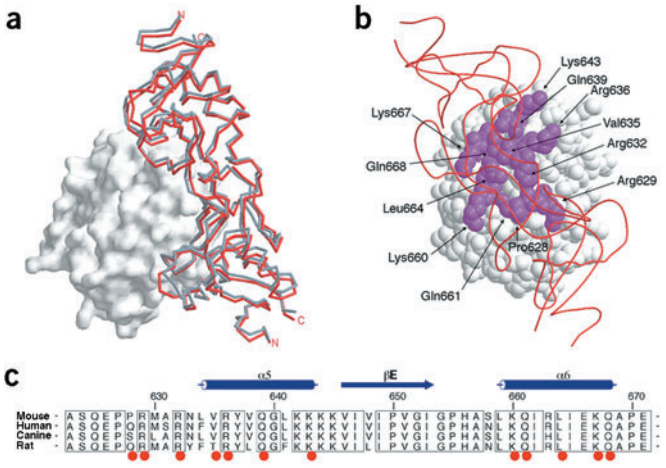

Figure 1 Structure and comparison of the mouse vWF-A1–botrocetin binary complex. (**a**) Comparison of the binary A1–botrocetin human and mouse complexes (A1, gray surface; botrocetin, gray and red Cα traces for the human and mouse complexes, respectively). (**b**) Locations of the contact residues of the mouse A1 involved in botrocetin binding. Botrocetin is shown in red coil models. (**c**) Sequence conservation of the A1 domain from four different species in the region involved in botrocetin binding. The mouse A1 domain shares high sequence identity with human (86%), canine (89%), and rat (89%). Residues involved in botrocetin binding are indicated by red circles. Secondary structure elements are above the sequence alignment.

packing between these helices and the central β-sheet cause the helices to pack 2.5 Å closer together, whereas α5 changes its tilt. Botrocetin compensates for these structural differences in several ways. First, the bilobar lectin fold allows for a small quaternary change between the two lobes to optimize packing with the A1 domain. Second, three tyrosines at the heart of the interface alter side chain and main chain dihedral angles. Third, some salt bridges are weakened or broken, whereas others are strengthened or created. In these ways, the overall architecture of the binary complex is well conserved between mouse and human, with an r.m.s. deviation of 0.88 Å for the 446 equivalent Cα atom pairs and a similar buried surface (1,580 Å^2 versus ~1,600 Å^2). Given the high level of sequence homology between mammalian species, it seems probable that similar small alterations in the botrocetin structure would allow tight complexes to be formed in most cases. It is also noteworthy that the mouse and human complexes crystallize in different space groups with very different crystal packing. Botrocetin occupies an almost identical position in the two binary complexes, suggesting that its location is a true energy minimum in the binary complex, and that the shift of botrocetin observed in the ternary complex (see below) is a consequence of GPIbα binding rather than a different crystal environment.

Structure of the human ternary complex

To determine the structure of the human ternary complex, we expressed the vWF-A1 binding domain of GPIbα using recombinant baculovirus technology. Our initial fragment, residues 1–289, forms a robust ternary complex[14] but did not diffract well enough for structural analysis. We suspected that the anionic region beyond residue 267, which is disorganized in most structures of GPIbα, was impairing the formation of high-quality cocrystals. Thus, a shorter construct, comprising residues 1–265, was generated, including the core leucine-rich repeat domain and three intrachain disulfide bonds. This protein also forms a stable ternary complex with a 1:1:1 stoichiometry with A1 and botrocetin, but crystallized in a form suitable for high-resolution analysis. We determined its structure at a resolution of 2.95 Å by molecular replacement (**Fig. 2**).

Overview of the ternary complex

Comparison of the human ternary complex with the human A1–botrocetin binary complex reveals a marked rigid-body slide and rotation of botrocetin around the surface of the A1 protein such that it makes

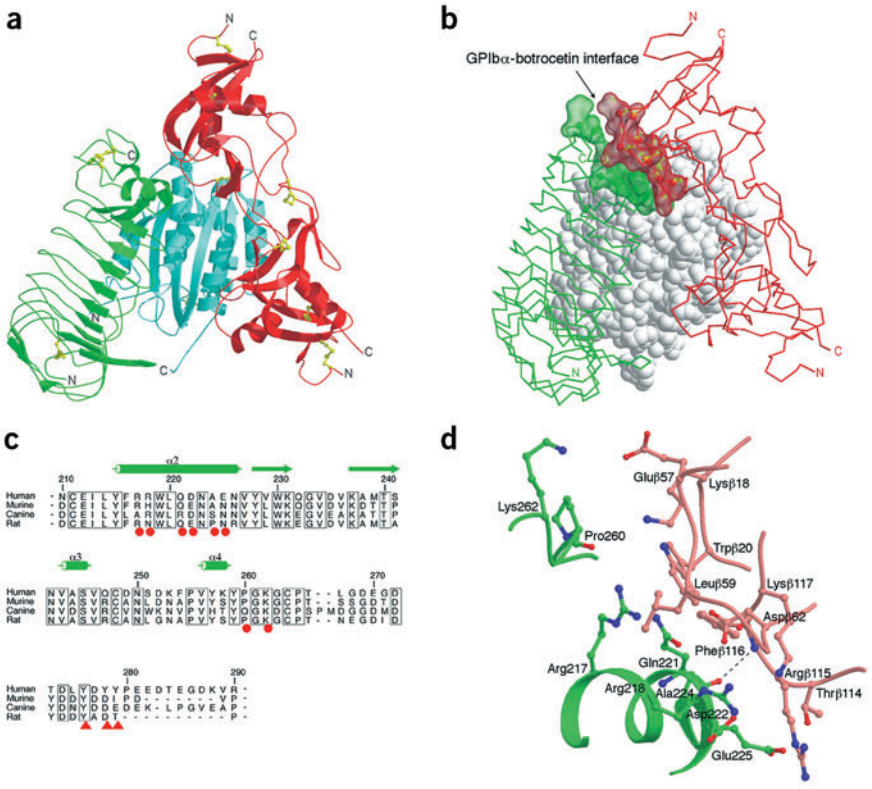

Figure 2 Structure of the vWF-A1–GPIbα–botrocetin ternary complex. (**a**) Ribbon representation of the ternary complex. vWF-A1, cyan; GPIbα, green; botrocetin, red. (**b**) Location of the GPIbα-botrocetin interface. The A1 domain, GPIbα, and botrocetin are in space-filling, green stick and red stick representations, respectively. The GPIbα-botrocetin interface is shown as green and red transparent surfaces. (**c**) Alignment of GPIbα sequences from four different species in the region involved in botrocetin binding (C-terminal to the leucine-rich repeat). The human receptor shares high sequence identity with mouse (68%), canine (65%), and rat (69%). Secondary structure elements are shown above the sequence alignment. Residues directly involved in the botrocetin interface are indicated by red circles. The tyrosine residues to be sulfated in human GPIbα are indicated by red arrows. Residues conserved in all the sequences are boxed. (**d**) Close-up of the GPIbα-botrocetin interface with backbone as ribbon and loop (GPIbα, green; botrocetin, pink), and selected side chains in ball-and-stick. An intermolecular main chain hydrogen bond is a dashed line.

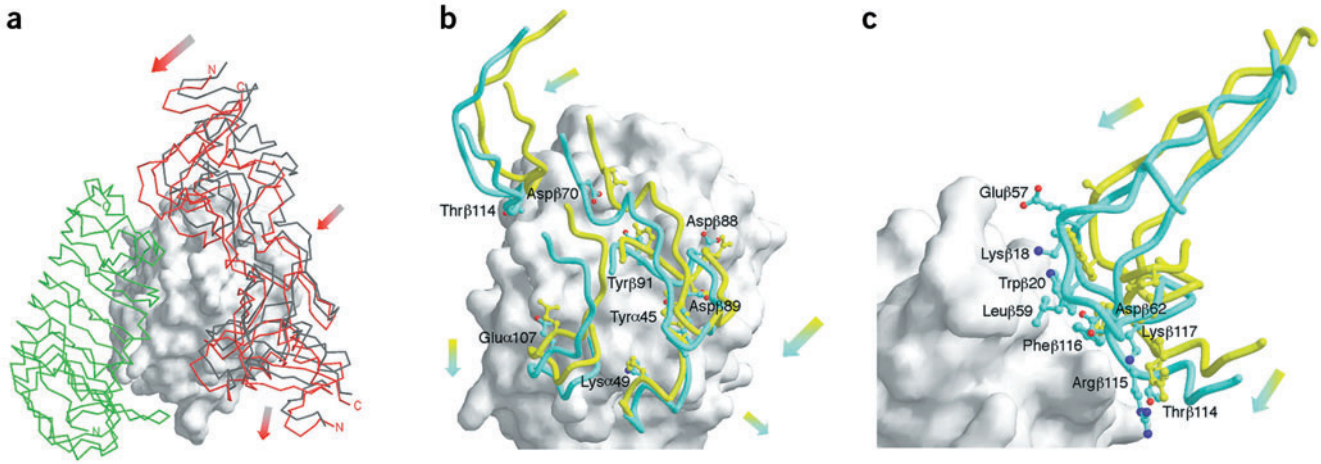

Figure 3 Structural changes on formation of ternary complex. (**a**) Overview showing the shift in botrocetin upon binding of GPIbα. Overlay is on the A1 domain. Botrocetin (Cα trace) is black and red in the binary and ternary complexes, respectively. GPIbα (Cα trace) is green, with a solvent-accessible surface of A1 in gray. Arrows show principal directions of motion. (**b**) Close-up of botrocetin in the binary (yellow coil) and ternary (cyan coil) complexes, with selected side chains shown, and the A1 domain shown as a solvent accessible surface. (**c**) Close-up comparison of botrocetin binary and ternary complexes in the region of the GPIbα-botrocetin interface (GPIbα shown as solvent-accessible surface).

a new interface with GPIbα (**Fig. 3**). The shift in center of gravity is 3.7 Å in a direction toward GPIbα, with movements of individual Cα atoms of as much as 10 Å at the N terminus of the β-chain. The location of GPIbα on the surface of A1 is similar to that in the previously reported A1–GPIbα binary complex (PDB entry 1M10)[12], although there is a ~1 Å rigid-body shift of GPIbα toward botrocetin.

The A1 domain in the ternary complex is essentially unchanged compared with its structure in the unliganded state (PDB entry 1AUQ)[15]. In particular, the N- and C-terminal arms are as well ordered as in the uncomplexed A1 domain, in contrast to the loss of order observed in binary A1–GPIbα complexes. We also did not observe a change in conformation of a loop on the lower surface of the A1 domain, as was reported in the wild-type binary complex (PDB entry 1SQ0)[16]; rather, it is identical to that seen in the mutant complex[12]. Thus, a botrocetin-induced conformational change in the A1 domain does not seem to contribute to its increased affinity for GPIbα. This result is consistent with our previous findings showing that the effects of botrocetin and type 2B vWD mutations (the latter is thought to destabilize the terminal arms of the A1 domain) are additive, suggesting distinct molecular mechanisms for affinity enhancement.

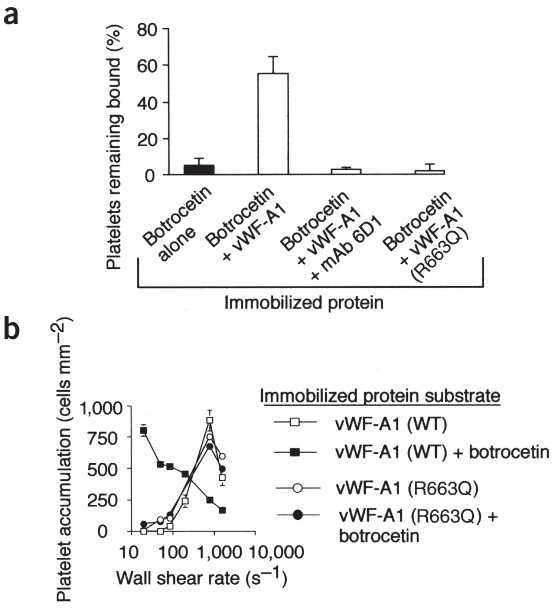

Figure 4 Requirement for botrocetin binding to the A1 domain. (**a**) The percentage of platelets capable of binding to mutant or wild-type (WT) vWF-A1 proteins in the absence or presence of botrocetin under static conditions. Purified cells were allowed to settle onto the indicated surface-immobilized protein substrates. After 10 min of contact, a wall shear stress of 0.2 dyn cm^{-2} was applied for 1 min, and the percentage of platelets that remained bound was determined (mean ± s.d., $n = 3$). (**b**) Accumulation of platelets per unit area on surface-absorbed mutant or WT vWF-A1 substrates at wall shear rates ranging from 20 to 1,600 s^{-1}. Error bar, s.d. for the mean values of three experiments carried out in duplicate.

Changes in the A1-botrocetin interface

The rigid-body movement of botrocetin in the ternary complex involves repacking of side chains at the A1-botrocetin interface (**Fig. 3a**,**b**). Two out of five salt bridges (using a distance cutoff of 3.5 Å) that occur within this region are disrupted when GPIbα binds, whereas in their place four new polar interactions are formed (Gln628–Aspβ70, Arg632–Thrβ114, Lys643–Leuα110 and Arg663–Aspβ88). Substantial repacking (shifts of 2–3 Å) of hydrophobic residues at the center of the interface also occurs. These changes actually lead to a higher shape correlation in the A1-botrocetin interface upon binding to GPIbα (0.52 versus 0.65). Furthermore, the overall buried surface area changes very little (1,620 $Å^2$ versus ~1,600 $Å^2$), so that the energetic cost of the repacking may be small enough that any loss can be recouped from the energetic gain arising from the new botrocetin–GPIbα interaction.

The new GPIbα-botrocetin interface

The new interface with GPIbα buries ~850 $Å^2$ of surface area (**Figs. 2** and **3**). It is smaller than the A1-GPIbα or A1-botrocetin interfaces, and its shape correlation (0.48) is lower than those of the former (0.59) and latter (0.65) in the ternary complex. This new interface provides a rationale for the enhanced binding of GPIbα to vWF-A1 (see below), whereas its relatively small size provides a rationale for the lack of bind-

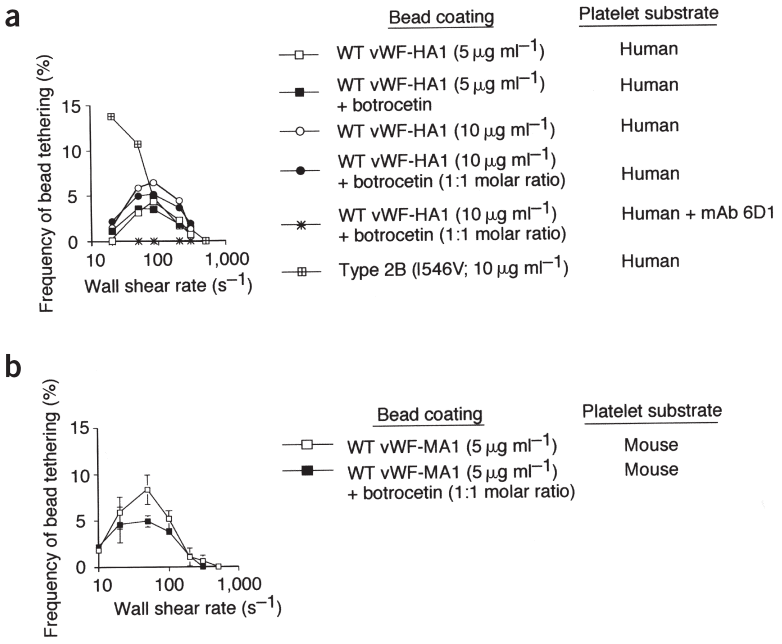

Figure 5 The effect of botrocetin on the kinetics of the GPIbα–vWF-A1 tether bond. (**a**,**b**) Botrocetin does not enhance the cellular on-rate for either the human or mouse GPIbα–vWF-A1 tether bond as observed for the type 2B mutation I546V. An enhancement in cellular on-rate is denoted as an increase in tethering frequency of protein-coated beads. Data represent mean ± s.d. for three independent experiments. WT, wild type.

ing observed between GPIbα and botrocetin in the absence of the A1 domain[17]. Three loops from botrocetin engage a flat surface comprising an α-helix and C-terminal strand that cap the C-terminal end of the leucine-rich repeat of GPIbα. At its center are loops containing Pheβ116 and Trpβ20 from botrocetin. Trpβ20 packs against polar side chains (Arg217 and Gln221), whereas Pheβ116 packs against a hydrophobic side chain of Ala224. A third loop (residues β55–60) from botrocetin that was disordered in the A1–botrocetin binary complex becomes ordered upon formation of the ternary complex (**Fig. 2d**) and makes contact with the C terminus. There are several long-range ionic interactions and one main chain–main chain hydrogen bond, between the carbonyl oxygen of Gln221 on GPIbα and the amide nitrogen of Pheβ116 on botrocetin.

Four GPIbα sequences are known: human[18], mouse[19], dog[20] and rat (NCBI entry XP_220573). They are 65–70% identical overall, less well conserved than the A1 domains, but similar enough to ensure that they will share a very similar three-dimensional structure. Within the region of GPIbα adjacent to the botrocetin-binding site, there is good conservation of buried residues (**Fig. 2c**), suggesting that the local main chain architecture will be conserved. Although the GPIbα interface residues are not as well conserved as those at the A1-botrocetin interface, there are no radical changes among the known mammalian GPIbα sequences, consistent with the ability of botrocetin to bind to GPIbα sequences of several species.

C-terminal to the leucine-rich repeat of GPIbα is an anionic region that includes three sulfated tyrosines (at residues 276, 278 and 279) in the human protein (not conserved in other species). Mutagenesis experiments have suggested a role for this region in botrocetin-dependent binding to human vWF[21,22], but definitive structural evidence is lacking. Although the construct that we analyzed crystallographically lacks this region, simple modeling based on the structure of this region observed in unliganded GPIbα (PDB entry 1GWB)[23] is consistent with the hypothesis that this region makes additional contacts with botrocetin in the ternary complex. We therefore measured the binding kinetics of our short and long recombinant GPIbα proteins to the A1–botrocetin binary complex using Biacore (data not shown). This revealed a six-fold increase in affinity when the anionic region was included. Thus, the anionic region seems to have a role in stabilizing the human ternary complex.

Prerequisite formation of the botrocetin–vWF-A1 complex

To show that botrocetin cannot form stable adhesions with platelets in the absence of the A1 domain, we evaluated platelet binding to surface-immobilized botrocetin under static conditions. After an incubation period of 10 min, few platelets remained attached upon the application of flow (**Fig. 4a**). By contrast, >50% of platelets remained bound in the presence of the botrocetin–vWF-A1 complex, but <5% remained bound when cells were first incubated with the GPIbα function-blocking antibody 6D1. To further show that botrocetin must form a complex with vWF-A1 to enhance interactions with platelets, a mutation was introduced into the A1 domain at the botrocetin interface that precludes the binding of this snake venom protein (R663Q). Although this mutation prevented botrocetin from stabilizing adhesion between the A1 protein and platelets either in stasis or under low-flow conditions, it did support a similar level of platelet accumulation at higher flow rates as compared with its wild-type counterpart (**Fig. 4a**,**b**).

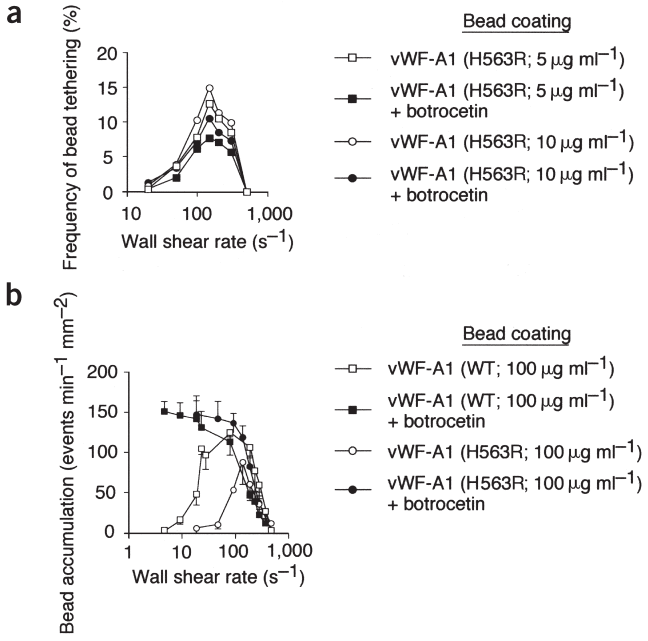

Figure 6 The botrocetin-GPIbα interface regulates the off-rate of the ternary complex. (**a**) The effect of botrocetin on the tethering frequency (apparent on-rate) of microspheres coated with low site densities of vWF-A1. (**b**) Accumulation of microspheres coated with a high concentration of vWF-A1 protein alone or in complex with botrocetin to surface-immobilized platelet monolayer under flow conditions. Data represent the mean ± s.d. for three independent experiments. WT, wild type.

Table 1 Off-rates as a function of wall shear stress

Shear stress (dyn cm^{-2})	vWF-HA1 (5 μg ml^{-1})		vWF-HA1 (5 μg ml^{-1}) + botrocetin		vWF-HA1 (10 μg ml^{-1}) + botrocetin		vWF-MA1 (5 μg ml^{-1})		vWF-MA1 (5 μg ml^{-1}) + botrocetin	
	k_{off}	R^2	k_{off}	R^2	k_{off}	R^2	k_{off}	R^2	k_{off}	R^2
0.85	5.88	0.98	1.74	0.98	1.79	0.98				
1.0	6.53	0.97	2.33	0.98	2.22	0.98	4.7	0.98	1.7	0.98
1.5	7.45	0.98	2.58	0.99	2.78	0.99				
2.0	8.07	0.97	2.79	0.99	2.99	0.99				
2.5			3.18	0.98	3.29	0.98				

Kinetics of dissociation of transiently tethered human (H) or mouse (M) A1-coated beads on surface-immobilized human or mouse platelets, respectively in the absence or presence of botrocetin (1:1 molar complex). Representative k_{off} values obtained for each experiment (minimum of four) are shown as a function of increasing wall shear stress.

Kinetics of the vWF-A1–GPIbα–botrocetin complex

We next analyzed the formation and dissociation of transient adhesive events, known as tether bonds, formed between microspheres coated with low site densities of vWF-A1 and surface-immobilized platelets. Previously, we have demonstrated the ability of this specialized flow system to elucidate the alteration in the intrinsic properties of the GPIbα–vWF-A1 tether bond that occurs upon the incorporation of function-enhancing mutations[24], obtaining results that were consistent with observed changes in structure[12]. By varying the bead coating concentration of vWF-A1, we found that at site densities between ~30 (5 μg ml^{-1}) and 52 (10 μg ml^{-1}) molecules μm^{-2}, transient tethering events are the predominant (>95%) adhesive interaction at wall shear rates ranging from 10 to 300 s^{-1}. Under these conditions, which limit the possibility of multiple bond formation, botrocetin does not increase the frequency of tether bond formation, indicating that botrocetin does not alter the on-rate[25,26] (**Fig. 5a**). That is, the rate of association closely resembles the normal physiological interaction between GPIbα and the A1 domain of vWF. Identical results were found for the mouse complex (**Fig. 5b**). This result is consistent with our structural data and modeling, which indicated that botrocetin does not alter the structure of the A1 domain and does not initially form contacts with GPIbα. This contrasts with gain-of-function mutations associated with type 2B vWD, which increase the association rate owing to structural changes that facilitate interactions between GPIbα and vWF-A1 (refs. 2,12,24).

The effect of botrocetin on the dissociation rate constant of the GPIbα–vWF-A1 tether bond was quantified by measurement of the duration of transient tethering events. High-temporal-resolution video analysis of the receptor-mediated bead-platelet interactions revealed that the interaction time distribution was exponential, in accordance with the hypothesis that a single GPIbα–vWF-A1 tether bond mediates adhesion (see Methods). Moreover, statistical point estimates (SPEs) of the tether bond dissociation constant (off-rate) k_{off} were consistent for all biological replicates ($P < 0.01$) at each wall shear stress. Graphically, this is manifested as a straight line in an exponential probability plot of the pause times (**Table 1**; see **Supplementary Fig. 1** online)[27–29].

To determine the intrinsic off-rate (that is, in the absence of an applied force), we (i) fit the SPEs of k_{off} to Bell's model[30], $k_{off}(F) = k_{off}(0)\exp(\sigma F_b / kT)$, via linear regression, and (ii) fit the experimental pause time distributions to a Bell model via the Monte Carlo (MC) simulation method[2,3]. Both fits were statistically significant ($P < 0.05$) and returned statistically indistinguishable results for both the zero-force off-rate k^0_{off} ($P << 0.01$) and 'reactive compliance' σ ($P << 0.01$) when applied to the same data (**Table 2**; see **Supplementary Fig. 2** online). Extrapolation to zero force yielded $k^0_{off} = 1.61 \pm 0.21$ s^{-1} and 1.72 ± 0.23 s^{-1} (mean ± s.e.) for vWF-A1 coating concentrations of 5 and 10 μg ml^{-1}, respectively, which are statistically indistinguishable ($P < 0.01$). Thus, in the absence of force, botrocetin increases the lifetime of the GPIbα–vWF-A1 tether bond two-fold (**Table 2**). We also evaluated the effect of botrocetin on tether bond formation between mouse vWF-A1 and mouse platelets. Notably, the results were nearly identical to those observed for the human binary complex, a ~2.5-fold reduction in the off-rate induced by botrocetin (**Table 1**, see **Supplementary Fig. 1** online). Thus, the mechanism of affinity regulation seems to be conserved across species.

The contribution of the botrocetin-GPIbα interface

To determine whether the prolongation in bond lifetime is due to the dissociation of the botrocetin-GPIbα interface, we evaluated the effect of botrocetin on the A1 mutant, H563R, which produces extremely labile interactions with GPIbα[31]. His563 is located in the middle of the strand C of the A1 domain, such that its side chain does not directly influence formation of the intermolecular β-sheet. However, once formed, the mutant complex may experience unfavorable ionic side chain interactions between the arginine side chain and Lys231 on GPIbα. Consistent with this, the mutation did not substantially alter the frequency of tether bond formation under conditions that limit multiple bond formation (bead coating concentrations ≤10 μg ml^{-1}), but did result in a 2.5-fold higher off-rate as compared with its wild-type counterpart in the absence of botrocetin (**Fig. 6a** and **Table 3**; see **Supplementary Fig. 3** online). In the presence of botrocetin, however, the binding of microspheres to surface-immobilized platelets was augmented at low flow rates (<20 s^{-1}) only when in a 1:1 molar ratio with high coating concentrations of mutant A1 (100 μg ml^{-1}), as observed for the wild-type binary complex (**Fig. 6b**). Evaluation of the impact of botrocetin on the frequency of transient tethers formed at low site densities of mutant vWF-A1 revealed no enhancement in on-rate, consistent with its lack of allosteric effect on this domain. It did, however, decrease the off-rate by five-fold to a value identical to the wild type A1 in the presence of botrocetin (2.2 ± 0.1 s^{-1} versus 2.2 ± 0.2 s^{-1}, mean ± s.d.). These observations indicate that the botrocetin-GPIbα interface, which would be relatively unperturbed in the mutant protein, must account for the similarities in off-rate and thus is rate-determining for the ternary complex (**Fig. 7**). Moreover, our data suggest that the motion of botrocetin around the A1 surface is relatively fast compared with the inherent bond lifetime of GPIbα–vWF-A1 interface, permitting sufficient time for botrocetin to interact with GPIbα.

Table 2 Biophysical parameters of the binary versus ternary complex

	k^0_{off} (s^{-1})	σ (nm)
vWF-A1 (without botrocetin)		
SPE	3.21 ± 0.15	0.018 ± 0.002
MCR	3.45 ± 0.37	0.016 ± 0.002
vWF-A1 (with botrocetin)		
SPE	1.62 ± 0.29	0.014 ± 0.005
MCR	1.61 ± 0.21	0.015 ± 0.003

Values for k^0_{off} were determined from regressions of data obtained from two independent analyses, MCR (Monte Carlo regression) and SPE. *P* values based on a two-tailed Student's *t*-test revealed no statistically significant differences in MCR- or SPE-derived values for k^0_{off}, and reactive compliance known as σ (a measure of a tether bond's sensitivity to force-driven dissociation); $P > 0.1$.

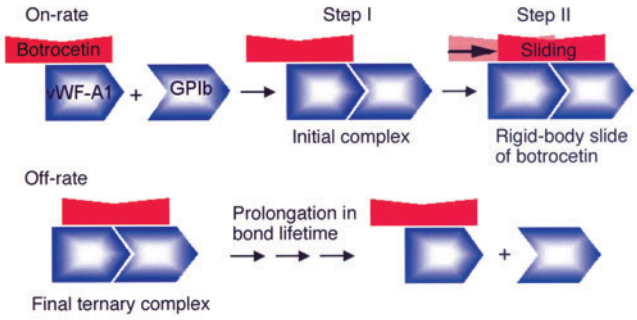

Figure 7 Proposed schematic model for the two-step mechanism of interaction between the botrocetin–vWF-A1 binary complex and GPIbα.

DISCUSSION

Although most toxins act by inhibiting biochemical processes, some are activators, either through binding to conserved surfaces and acting as allosteric effectors that stabilize one quaternary conformation of their target[32], or by enzymatically modifying their targets[33]. However, the manner in which botrocetin enhances GPIbα–vWF-A1 interactions, by creating an additional interface, seems to be unprecedented. A priori, such a mechanism places great demands on the positioning of botrocetin on the A1 surface (in contrast with steric inhibition of protein-protein interactions, for which the structural requirements are much less severe). Botrocetin achieves this using three elements. First, it binds to a conserved surface on the A1 domain adjacent to but not interfering with the GPIbα-binding site, as shown by the unchanged on-rate for GPIbα and consistent with model building based on the binary complexes. Second, the inherent flexibility of the A1-botrocetin binding interface allows botrocetin to slide rapidly over the A1 surface to form a new interface with GPIbα. Third, botrocetin presents a hydrophobic but not highly specific interface for interaction with a conserved though not invariant region of GPIbα, which dictates the bond dissociation rate.

Why does botrocetin undergo such a slide, rather than initially assuming its position in the ternary complex? One possibility is that a sliding mechanism avoids steric crowding that occurs near the interface where the three molecules must come into apposition. In particular, this 'trimolecular' interface occurs at the base of the 'β-switch' region of GPIbα, which undergoes a disorder-order transition from loop to a rigid β-hairpin that forms the major part of the β-sheet interaction at the top of the A1 domain. Indeed, it is known that the on-rate for binding to the A1 domain is highly sensitive to mutations that affect the propensity for β-strand formation in this region[12]. We propose that the presence of botrocetin at its 'ternary' location would adversely affect the ability of the β-switch to undergo the necessary conformational changes required to form a hairpin and sheet. By contrast, botrocetin's subsequent slide is a simple rigid-body motion to form the new interface with GPIbα. The two-step mechanism may also provide the adaptability necessary to overcome structural differences in various mammalian species that lead to subtle variations in the position and orientation of botrocetin on the surface of vWF-A1 before binding GPIbα. Thus, we propose that the two-step mechanism avoids an adverse effect on the on-rate that would limit botrocetin's effectiveness as a snake venom protein.

It may seem surprising that a two-fold decrease in the off-rate is sufficient for the strong biological effect observed for botrocetin. However, such subtle alterations in kinetics have been shown to have profound effects in other cellular contexts. For example, it has been postulated that the kinetics of T-cell receptor (TCR) binding to peptide–major histocompatibility complexes (MHCs) must be maintained within an extremely narrow range to promote T-cell activation. In fact, only a two-fold difference in the lifetime of this interaction has been reported to result in a marked alteration in T-cell responsiveness to a peptide–MHC complex[34]. In regard to botrocetin, we believe that the observed two-fold prolongation of bond lifetime is also sufficient to contribute to the clinical phenotype that results from envenomation by *B. jararaca*[6]. This is supported by the ability of botrocetin, in combination with high but not limiting concentrations of A1 on beads, to augment binding in low-flow states, a phenomenon we believe to rely on multiple bond formation[35]. By prolonging the off-rate, the probability of forming more than one GPIbα–vWF-A1 interaction increases markedly, an event that would favor stabilization of platelet-vWF aggregates. Moreover, because the venom of *B. jararaca* contains several procoagulant proteins that would augment the effects of botrocetin, a modest alteration in the dissociation rate constant may be all that is required to achieve the desired pathological effect, hemorrhage.

Table 3 The effect of botrocetin on k_{off} for extremely labile tether bonds

Shear stress	vWF-HA1 (H563R)		vWF-HA1 (H563R) + botrocetin		vWF-HA1 (WT) + botrocetin	
(dyn cm^{-2})	k_{off}	R^2	k_{off}	R^2	k_{off}	R^2
1.0	15.4	0.99	2.3	0.97	2.3	0.99

Kinetics of dissociation of transiently tethered mutant vWF-A1-coated beads on surface-immobilized platelets in the absence or presence of botrocetin (1:1 molar complex). Representative k_{off} values obtained for each experiment (minimum of four) are shown in comparison with wild-type (WT) vWF-A1 that is in complex with botrocetin at 1 dyn cm^{-2} of wall shear stress.

METHODS

Reagents and antibodies. Monoclonal antibodies (mAbs) used in experiments included GPIbα blocking mAb 6D1, mAb 7E3 specific to human $\alpha_{IIb}\beta_3$(from B. Coller, Rockefeller University), mAb NAD-1 specific to mouse $\alpha_{IIb}\beta_3$ (ref. 36) and mouse antibody to His_6-tag. The generation of Fab fragments, recombinant human and mouse vWF-A1 His-tagged proteins, coating of latex microspheres (7-μm diameter) and purification of botrocetin from the crude venom of *B. jararaca* were carried out as described[2,8,37–39].

Platelet adhesion in flow. Platelets purified from healthy donors were perfused (5×10^7 ml^{-1}, Tyrode's buffer, 0.25% (v/v) human serum albumin, pH 7.4) over surface-immobilized vWF-A1 proteins (100 μg ml^{-1}) in a parallel plate flow chamber at various wall shear rates (20–1,600 s^{-1}) and their attachment recorded as described[2]. For experiments involving botrocetin, A1 domain proteins were incubated with the purified snake venom (1:1 molar ratio) for 30 min at room temperature. Inhibition studies were done by incubating platelets with mAb 6D1 (20 μg ml^{-1}) for 15 min at ambient temperature before adhesion studies. In experiments involving the adhesion of platelets to botrocetin–vWF-A1 substrates under stasis, platelets (2×10^7 ml^{-1}) that had been initially perfused through a parallel plate flow chamber at 0.5 dyn cm^{-2} for 30 s were allowed to remain in close proximity with the substrate for 10 min before reinstatement of flow at 0.2 dyn cm^{-2}. The number of cells remaining bound after the application of flow for 1 min was determined and expressed as the percentage of the original number of platelets present in the field of view (0.32 mm^2).

Microsphere tethering frequency. In flow experiments involving vWF-A1-coated microspheres, purified platelets pretreated with 10 mM sodium azide, 50 ng ml^{-1} prostaglandin E_1 and 10 μM indomethacin (Sigma) were immobilized on glass plates coated with Fab 7E3 (for human) or Fab NAD-1 (for mouse) fragment as described[24]. The frequency of tethering events between the platelet substrate and microspheres coated with a low site density of vWF-A1 was measured by determining the number of beads that paused, but did not translocate, at shear rates ranging from 20 to 500 s^{-1} to ascertain any perturbations in cellular on-rate. This value was then normalized by dividing the number of beads that formed tran-

Table 4 Data collection and refinement statistics

	Human A1–GPIbα–botrocetin	Mouse A1–botrocetin
Data collection		
Space group	$P4_12_12$	$P2_12_12_1$
Cell dimensions		
a, *b*, *c* (Å)	108.3, 108.3, 220.0	56.3, 73.7, 114.4
Resolution (Å)	200–2.95 (3.0–2.95)	200–2.7 (2.75–2.7)
R_{merge}	0.099 (0.347)	0.089 (0.284)
$I / \sigma I$	16.7 (3.1)	16.1 (2.5)
Completeness (%)	94.6 (87.9)	92.4 (79.6)
Redundancy	6.5 (3.2)	4.2 (2.4)
Refinement		
Resolution (Å)	6.0–2.95	6.0–2.7
Number of reflections	23,643	11,310
R_{work} / R_{free}	0.213 / 0.276	0.218 / 0.288
No. atoms		
Protein	5,864	3,689
Water	0	39
B-factors (Å^2)		
Protein	48.79	41.10
Water	–	35.56
R.m.s. deviations		
Bond lengths (Å)	0.007	0.008
Bond angles (°)	1.4	1.4

sient tethers by the number of noninteracting beads transported across the field of view in the focal plane of the immobilized protein substrate. In experiments involving botrocetin, vWF-A1-coated beads (2×10^6 ml^{-1}) were incubated with botrocetin (1:1 molar ratio) for 30 min with agitation at ambient temperature. The amount of vWF-A1 coupled to beads was estimated as described[2]. The site density of vWF-A1 on beads coated with 5 μg ml^{-1} of protein was estimated to be ~30 sites μm^{-2}.

Dissociation rate constants and mechanical strength of transient tethers. The duration of transient tethers was estimated for vWF-A1-coated microspheres interacting with surface-immobilized platelets (a total platelet coverage of <10%) at wall shear stresses ranging from 0.85 to 2.5 dyn cm^{-2}, as described[2,24]. Only one tethering event per bead was counted during the observation period. The duration of these interactions was measured by recording images from a Nikon X60 DIC objective (oil immersion) viewed at a frame rate of 235 frames s^{-1}. We recorded 30–50 interact pause times (duration of interactions) for each pool (at least four) of surface-bound platelets and wall shear stress. If a single tether bond mediates adhesion between beads and cells, its duration is exponentially distributed with mean $1 / k_{off}$, where k_{off} is its dissociation rate constant[40]. Moreover, a plot of the cumulative distribution of pause times appears linear on semilog axes. Hence, the SPE for k_{off} was $k_{off} = <t>^{-1}$, where $<t>$ is the average duration. The force-dependence of k_{off} was determined by linear regression of $\ln(k_{off})$ to the force applied to the bond (F_b) in accordance with Bell's model, where F_b is computed from τ_ω as described[2,24]. The slope of the best-fit line is equal to σ / kT, where σ is the 'reactive compliance' and the intercept is $\ln(k^0_{off})$. Results are reported as mean ± s.e.

Monte Carlo simulation. If multiple tether bonds mediate adhesion, the pause time distribution depends on the rate of bond formation, k_{on}, and the surface densities of adhesive ligands, in addition to the dissociation rate, k_{off}. Pause time distributions resulting from both formation and dissociation of adhesive bonds were stochastically simulated via Gillespie's algorithm and optimized to fit the experimental observations as described[2,24,41].

Statistical analysis. A Student's *t*-test was used to determine the consistency of biological replicates at each τ_ω, the equality of Bell parameters (± botrocetin), and the quality of the Bell fit to SPEs (hypotheses $\sigma = 0$ and $R^2 = 0$). The adherence of the experimental pause time distributions to the 'single bond' and 'multibond' pause time distributions intrinsic to the SPE and MC approaches was evaluated via the Kolmogorov-Smirnov test for each biological replicate and wall shear stress. Values of $P < 0.05$ were considered significant for the rejection of null hypotheses.

GPIbα production and complex formation. Recombinant human GPIbα protein (N21Q and N159Q) was expressed in baculovirus-infected insect cells. Briefly, DNA encoding a Kozak sequence[42], the signal sequence and extracellular region of GPIbα (residues –16 to 265)[18] followed by C-terminal thrombin cleavage site and His_6-tag was subcloned into pFastBac1 (Life Technologies). Recombinant baculovirus was generated using Bac-to-Bac system (Invitrogen) according to the manufacturer's instructions, and the virus was used to infect Sf9 insect cells for expression of GPIbα. Soluble secreted GPIbα was purified from the culture supernatant using nickel affinity chromatography followed by RESOURCE PHE hydrophobic chromatography (Amersham Biosciences). The protein was dialyzed in 20 mM Tris-HCl, pH 8, and 150 mM NaCl, and the His-tag was cleaved by bovine thrombin (Amersham Biosciences) at room temperature.

Limited proteolysis of the A1 proteins was carried out for crystallization experiments as described[15]. The human A1–botrocetin binary complex was generated as described[11] and incubated with GPIbα in 20 mM Tris-HCl, pH 8, and 150 mM NaCl for 30 min at room temperature. The ternary complex was purified by a Superdex 200 column (Amersham Biosciences), which yielded a single peak at a molecular mass of ~84 kDa, consistent with the total molecular mass of the ternary complex. The mouse A1–botrocetin binary complex was generated and purified as described for the human complex[11].

Crystallization and structure determination. Crystals of the ternary complex (human A1–GPIbα–botrocetin) were grown at 4 °C in sitting drops by mixing equal volumes of protein complex (11 mg ml^{-1}) and reservoir consisting of 0.1 M sodium HEPES, pH 7.5, 1.0 M sodium citrate and 20 mM L-cysteine. X-ray diffraction data were collected at 100 K using a Rigaku RU300 generator ($\lambda = 1.5418$ Å) and R-AXIS IV image plate detector. The crystals belong to space group $P4_12_12$, with one ternary complex per asymmetric unit. Crystals of the binary complex (mouse A1–botrocetin) were grown at room temperature in hanging drops by mixing equal volumes of protein complex (4.6 mg ml^{-1}) and reservoir solution consisting of 0.1 M sodium cacodylate, pH 6.5, 13% (w/v) PEG 5000 monomethyl ether and 0.2 M sodium sulfate. Data were collected at 100 K at beamline 7-1 ($\lambda = 1.08$ Å) at Stanford Synchrotron Radiation Laboratory using a MAR 345 image plate detector. The crystals belong to space group $P2_12_12_1$ with one binary complex per asymmetric unit. All data were processed and scaled using the HKL package[43] (**Table 4**).

The structures were solved by molecular replacement with AmoRe[44]. The search models were the human A1–botrocetin complex (PDB entry 1IJK)[11] and GPIbα (PDB entry 1M0Z)[12] for the A1–GPIbα–botrocetin ternary complex; the human A1 (PDB entry 1AUQ)[15] and botrocetin (PDB entry 1FVU)[45] for the mouse A1–botrocetin complex. Model building was done using TURBO-FRODO[46]. Initial models were subjected to rigid-body refinement followed by positional and simulated-annealing refinements using CNS[47]. Data collection and refinement statistics are summarized in **Table 4**. Stereochemistry of the structures was assessed by PROCHECK[48]. Shape correlation statistics were calculated using Sc[49]. Figures were prepared using MolScript[50], Raster3D[51], GRASP[52] and ALSCRIPT[53].

Coordinates. The coordinates of the ternary complex (human vWF-A1–GPIbα–botrocetin) and the binary complex (mouse vWF-A1–botrocetin) have been deposited in the Protein Data Bank (accession codes 1U0N and 1U0O, respectively).

Note: Supplementary information is available on the Nature Structural & Molecular Biology website.

ACKNOWLEDGMENTS

We thank to the staff of the Stanford Synchrotron Radiation Laboratory and the US Department of Energy for the use of X-ray data collection facilities. This work was supported by grants from the US National Institutes of Health (to R.C.L and T.G.D), the American Heart Association (T.G.D.) and a postdoctoral fellowship from the PhRMA Foundation (I.J.L.).

COMPETING INTERESTS STATEMENT
The authors declare that they have no competing financial interests.

Received 17 September 2004; accepted 6 December 2004
Published online at http://www.nature.com/nsmb/

1. Savage, B., Almus-Jacobs, F. & Ruggeri, Z.M. Specific synergy of multiple substrate-receptor interactions in platelet thrombus formation under flow. *Cell* **94**, 657–666 (1998).
2. Doggett, T.A. *et al.* Selectin-like kinetics and biomechanics promote rapid platelet adhesion in flow: the GPIbα-vWF tether bond. *Biophys. J.* **83**, 194–205 (2002).
3. Kumar, R.A. *et al.* Kinetics of GPIbα–vWF-A1 tether bond under flow: effect of GPIbα mutations on the association and dissociation rates. *Biophys. J.* **85**, 4099–4109 (2003).
4. Read, M.S., Shermer, R.W. & Brinkhous, K.M. Venom coagglutinin: an activator of platelet aggregation dependent on von Willebrand factor. *Proc. Natl. Acad. Sci. USA* **75**, 4514–4518 (1978).
5. Brinkhous, K.M., Read, M.S., Fricke, W.A. & Wagner, R.H. Botrocetin (venom coagglutinin): reaction with a broad spectrum of multimeric forms of factor VIII macromolecular complex. *Proc. Natl. Acad. Sci. USA* **80**, 1463–1466 (1983).
6. Sanders, W.E., Read, M.S., Reddick, R.L., Garris, J.B. & Brinkhous, K.M. Thrombotic thrombocytopenia with von Willebrand factor deficiency induced by botrocetin. An animal model. *Lab. Invest.* **59**, 443–452 (1988).
7. Fujimura, Y., Holland, L.Z., Ruggeri, Z.M. & Zimmerman, T.S. The von Willebrand factor domain-mediating botrocetin-induced binding to glycoprotein Ib lies between Val449 and Lys728. *Blood* **70**, 985–988 (1987).
8. Andrews, R.K., Booth, W.J., Gorman, J.J., Castaldi, P.A. & Berndt, M.C. Purification of botrocetin from *Bothrops jararaca* venom. Analysis of the botrocetin-mediated interaction between von Willebrand factor and the human platelet membrane glycoprotein Ib–IX complex. *Biochemistry* **28**, 8317–8326 (1989).
9. Rabinowitz, I. *et al.* von Willebrand disease type B: a missense mutation selectively abolishes ristocetin-induced von Willebrand factor binding to platelet glycoprotein Ib. *Proc. Natl. Acad. Sci. USA* **89**, 9846–9849 (1992).
10. Ajzenberg, N., Ribba, A.-S., Rastegar-Lari, G., Meyer, D. & Baruch, D. Effect of recombinant von Willebrand factor reproducing type 2B or type 2M mutations on shear-induced platelet aggregation. *Blood* **95**, 3796–3803 (2000).
11. Fukuda, K. *et al.* Structural basis of von Willebrand factor activation by the snake toxin botrocetin. *Structure* **10**, 943–950 (2002).
12. Huizinga, E.G. *et al.* Structures of glycoprotein Ibα and its complex with von Willebrand factor A1 domain. *Science* **297**, 1176–1179 (2002).
13. Jenkins, P.V., Pasi, K.J. & Perkins, S.J. Molecular modeling of ligand and mutation sites of the type A domains of human von Willebrand factor and their relevance to von Willebrand's disease. *Blood* **91**, 2032–2044 (1998).
14. Miura, S. *et al.* Interaction of von Willebrand factor A1 with platelet glycoprotein Ibα (1–289). Slow intrinsic binding kinetics mediate rapid platelet adhesion. *J. Biol. Chem.* **275**, 7539–7546 (2000).
15. Emsley, J., Cruz, M., Handin, R. & Liddington, R. Crystal structure of the von Willebrand factor A1 domain and implications for the binding of platelet glycoprotein Ib. *J. Biol. Chem.* **273**, 10396–10401 (1998).
16. Dumas, J.J. *et al.* Crystal structure of the wild-type von Willebrand factor A1–glycoprotein Ibα complex reveals conformational differences with a complex bearing von Willebrand disease mutations. *J. Biol. Chem.* **279**, 23327–23334 (2004).
17. Lo Conte, L., Chothia, C. & Janin, J. The atomic structure of protein-protein recognition sites. *J. Mol. Biol.* **285**, 2177–2198 (1999).
18. López, J.A. *et al.* Cloning of the α chain of human platelet glycoprotein Ib: a transmembrane protein with homology to leucine-rich α2-glycoprotein. *Proc. Natl. Acad. Sci. USA* **84**, 5615–5619 (1987).
19. Ware, J., Russell, S. & Ruggeri, Z.M. Cloning of the murine platelet glycoprotein Ibα gene highlighting species-specific platelet adhesion. *Blood Cells Mol. Dis.* **23**, 292–301 (1997).
20. Kenny, D., Morateck, P.A., Fahs, S.A., Warltier, D.C. & Montgomery, R.R. Cloning and expression of canine glycoprotein Ibα. *Thromb. Haemost.* **82**, 1327–1333 (1999).
21. Marchese, P. *et al.* Identification of three tyrosine residues of glycoprotein Ibα with distinct roles in von Willebrand factor and α-thrombin binding. *J. Biol. Chem.* **270**, 9571–9578 (1995).
22. Dong, J.-f. *et al.* Tyrosine sulfation of glycoprotein Ibα. Role of electrostatic interactions in von Willebrand factor binding. *J. Biol. Chem.* **276**, 16690–16694 (2001).
23. Uff, S., Clemetson, J.M., Harrison, T., Clemetson, K.J. & Emsley, J. Crystal structure of the platelet glycoprotein Ibα N-terminal domain reveals an unmasking mechanism for receptor activation. *J. Biol. Chem.* **277**, 35657–35663 (2002).
24. Doggett, T. *et al.* Alterations in the intrinsic properties of the GPIbα-VWF tether bond define the kinetics of the platelet-type von Willebrand disease mutation, Gly233Val. *Blood* **102**, 152–160 (2003).
25. Chang, K.-C. & Hammer, D.A. The forward rate of binding of surface-tethered reactants: effect of relative motion between two surfaces. *Biophys. J.* **76**, 1280–1292 (1999).
26. Chen, S. & Springer, T.A. Selectin receptor-ligand bonds: formation limited by shear rate and dissociation governed by the Bell model. *Proc. Natl. Acad. Sci. USA* **98**, 950–955 (2001).
27. Alon, R., Hammer, D.A. & Springer, T.A. Lifetime of the P-selectin-carbohydrate bond and its response to tensile force in hydrodynamic flow. *Nature* **374**, 539–542 (1995).
28. Ramachandran, V. *et al.* Tyrosine replacement in P-selectin glycoprotein ligand-1 affects distinct kinetic and mechanical properties of bonds with P- and L-selectin. *Proc. Natl. Acad. Sci. USA* **96**, 13771–13776 (1999).
29. Smith, M.J., Berg, E.L. & Lawrence, M.B. A direct comparison of selectin-mediated transient adhesive events using high temporal resolution. *Biophys. J.* **77**, 3371–3383 (1999).
30. Bell, G.I. Models for the specific adhesion of cells to cells. *Science* **200**, 618–627 (1978).
31. Bonnefoy, A. *et al.* Shielding the front-strand β3 of the von Willebrand factor A1 domain inhibits its binding to platelet glycoprotein Ibα. *Blood* **101**, 1375–1383 (2003).
32. Cestele, S. & Catterall, W.A. Molecular mechanisms of neurotoxin action on voltage-gated sodium channels. *Biochimie* **82**, 883–892 (2000).
33. Lerm, M., Schmidt, G. & Aktories, K. Bacterial protein toxins targeting rho GTPases. *FEMS Microbiol. Lett.* **188**, 1–6 (2000).
34. Matsui, K., Boniface, J.J., Steffner, P., Reay, P.A. & Davis, M.M. Kinetics of T-cell receptor binding to peptide/I-E^k complexes: correlation of the dissociation rate with T-cell responsiveness. *Proc. Natl. Acad. Sci. USA* **91**, 12862–12866 (1994).
35. Dwir, O. *et al.* Avidity enhancement of L-selectin bonds by flow: shear-promoted rotation of leukocytes turn labile bonds into functional tethers. *J. Cell Biol.* **163**, 649–659 (2003).
36. Chen, J., Diacovo, T.G., Grenache, D.G., Santoro, S.A. & Zutter, M.M. The α2 integrin subunit-deficient mouse: a multifaceted phenotype including defects of branching morphogenesis and hemostasis. *Am. J. Pathol.* **161**, 337–344 (2002).
37. Kahn, M.L. *et al.* Glycoprotein V-deficient platelets have undiminished thrombin responsiveness and do not exhibit a Bernard-Soulier phenotype. *Blood* **94**, 4112–4121 (1999).
38. Fujimura, Y. *et al.* Isolation and chemical characterization of two structurally and functionally distinct forms of botrocetin, the platelet coagglutinin isolated from the venom of *Bothrops jararaca*. *Biochemistry* **30**, 1957–1964 (1991).
39. Sekiya, F., Atoda, H. & Morita, T. Isolation and characterization of an anticoagulant protein homologous to botrocetin from the venom of *Bothrops jararaca*. *Biochemistry* **32**, 6892–6897 (1993).
40. Hammer, D.A. & Apte, S.M. Simulation of cell rolling and adhesion on surfaces in shear flow: general results and analysis of selectin-mediated neutrophil adhesion. *Biophys. J.* **63**, 35–57 (1992).
41. Gillespie, D.T. A general method for numerically simulating the stochastic time evolution of coupled chemical reactions. *J. Comput. Phys.* **22**, 403–434 (1976).
42. Afshar-Kharghan, V., Li, C.Q., Khoshnevis-Asl, M. & López, J.A. Kozak sequence polymorphism of the glycoprotein (GP) Ibα gene is a major determinant of the plasma membrane levels of the platelet GP Ib–IX–V complex. *Blood* **94**, 186–191 (1999).
43. Otwinowski, Z. & Minor, W. Processing of X-ray diffraction data collected in oscillation mode. *Methods Enzymol.* **276**, 307–327 (1997).
44. Navaza, J. AMoRe: an automated package for molecular replacement. *Acta Crystallogr. A* **50**, 157–163 (1994).
45. Sen, U. *et al.* Crystal structure of the von Willebrand factor modulator botrocetin. *Biochemistry* **40**, 345–352 (2001).
46. Roussel, A. & Cambileau, C. TURBO-FRODO. In *Silicon Graphics Geometry* (Silicon Graphics, Mountain View, California, USA, 1991).
47. Brünger, A.T. *et al.* Crystallography & NMR system: a new software suite for macromolecular structure determination. *Acta Crystallogr. D* **54**, 905–921 (1998).
48. Laskowski, R.A., MacArthur, N.W., Moss, D.S. & Thornton, J.M. PROCHECK: a program to check stereochemical quality of protein structures. *J. Appl. Crystallogr.* **26**, 283–291 (1993).
49. Lawrence, M.C. & Colman, P.M. Shape complementarity at protein/protein interfaces. *J. Mol. Biol.* **234**, 946–950 (1993).
50. Kraulis, P.J. MOLSCRIPT: a program to produce both detailed and schematic plots of protein structures. *J. Appl. Crystallogr.* **24**, 946–950 (1991).
51. Merritt, E.A. & Bacon, D.J. Raster3D: photorealistic molecular graphics. *Methods Enzymol.* **277**, 505–524 (1997).
52. Nicholls, A., Sharp, K.A. & Honig, B. Protein folding and association: insights from the interfacial and thermodynamic properties of hydrocarbons. *Proteins* **11**, 281–296 (1991).
53. Barton, G.J. ALSCRIPT: a tool to format multiple sequence alignments. *Protein Eng.* **6**, 37–40 (1993).